

Regular Article - Experimental Physics

# Photo-response of the N = Z nucleus <sup>28</sup>Si below 13.0 MeV

M. Scheck<sup>1,2,a</sup>, R. Schwengner<sup>3</sup>, O. Agar<sup>1,2,4</sup>, R. Beyer<sup>3</sup>, R. Chapman<sup>1,2</sup>, K. Gladnishki<sup>5</sup>, R.-D. Herzberg<sup>6</sup>, H. Hoffmann<sup>7</sup>, A. R. Junghans<sup>3</sup>, D. Kocheva<sup>5</sup>, S. E. Müller<sup>3</sup>, D. O'Donnell<sup>1,2</sup>, G. Rainovski<sup>5</sup>, K. Römer<sup>3</sup>, D. Savran<sup>8</sup>, K. Schmidt<sup>3</sup>, P. G. Thirolf<sup>9</sup>, A. Wagner<sup>3</sup>, O. Wieland<sup>10</sup>, A. Yadav<sup>3</sup>, F. Zhu<sup>6</sup>

- <sup>1</sup> School of Computing, Engineering, and Physical Sciences, University of the West of Scotland, Paisley PA1 2BE, UK
- <sup>2</sup> SUPA, Scottish Universities Physics Alliance, Glasgow, UK
- <sup>3</sup> Helmholtz-Zentrum Dresden-Rossendorf, 01328 Dresden, Germany
- <sup>4</sup> Department of Physics, Karamanoglu Mehmetbey University, Karaman, Turkey
- <sup>5</sup> Faculty of Physics, St. Kliment Ohridski University of Sofia, 1164 Sofia, Bulgaria
- <sup>6</sup> Department of Physics, Oliver Lodge Laboratory, University of Liverpool, Liverpool L69 7ZE, UK
- <sup>7</sup> Technische Universität Dresden, Institut für Kern- und Teilchenphysik, 01062 Dresden, Germany
- <sup>8</sup> GSI Helmholtzzentrum f
  ür Schwerionenforschung GmbH, 64291 Darmstadt, Germany
- <sup>9</sup> Ludwig-Maximilians-Universität München, 85748 Garching, Germany
- <sup>10</sup> INFN, Sezione di Milano, 20133 Milan, Italy

Received: 11 April 2025 / Accepted: 10 July 2025 © The Author(s) 2025 Communicated by Catalin Matei

**Abstract** The electric E1 and magnetic M1 dipole responses of the N=Z nucleus <sup>28</sup>Si were investigated in a nuclear resonance fluorescence experiment at the ELBE accelerator of the Helmholtz Zentrum Dresden-Rossendorf. The investigated energy range extends to 13.0 MeV, which corresponds to the kinetic energy of the electrons that were used to produce the unpolarised bremsstrahlung in the entrance channel of the  ${}^{28}\text{Si}(\gamma, \gamma')$  reaction. The bremsstrahlung photons excited three  $J^{\pi} = 1^{-}$ , seven  $J^{\pi} = 1^{+}$ , and several  $J^{\pi} = 2^{+}$  states. De-excitation  $\gamma$  rays were detected using the four high-purity germanium detectors of the  $\gamma$ ELBE setup. The excellent background conditions allowed to identify nine previously unobserved  $\gamma$ -ray transitions. In the investigated energy region of up to 13.0 MeV a total  $\sum_i B(M1, 0^+ \rightarrow$  $1_i^+) = 5.0(3) \ \mu_N^2$  strength is firmly observed with a possible addition of  $B(M1, 0^+ \rightarrow 1_i^+) \leq 0.14 \ \mu_N^2$  from levels for which the data allows to establish only an upper limit. Furthermore, below 13 MeV this N = Z nucleus exhibits a marginal isoscalar E1 strength of  $\sum_i B(E1, 0^+ \rightarrow 1^-) =$  $2.6(3) \times 10^{-3} \text{ e}^2 \text{fm}^2$ , which exhausts only 0.026(2) % of the energy-weighted sum rule.

## 1 Introduction

Published online: 12 August 2025

As evidenced by peaks found at mass numbers  $A = 4n(3 \le n \le 10)$  in the elemental abundance observed in the solar

system, nuclei composed of an integer number of  $\alpha$  particles are favorably synthesised when compared to other nuclei. In a stellar environment the  $(p, \gamma)$  proton-capture and  $(\alpha, \gamma)$  $\alpha$ -capture reactions will dominate the formation processes for light nuclei [1,2]. The capture of an  $\alpha$  particle from the  $J^{\pi} = 0^+$  ground state of an even-even nucleus prefers low momentum transfer and natural parity for the final state in the newly formed nucleus [3]. An increasing angular momentum transfer adds the corresponding centrifugal barrier to the Coulomb barrier, which results in a reduction of the reaction probability, consequently, levels with higher spins are increasingly suppressed. Hence, this reaction is dominated by channels ending in levels with natural spin and parity of  $J^{\pi} = 0^+, 1^-, 2^+$ . In proton-capture, the spin range of the capture state is given by  $J_0 \pm (l \pm 1/2)$ , where  $J_0$  is the ground-state spin of the capturing nucleus, 1/2 is the spin of the proton, and l the angular momentum of the partial wave of the incident proton. The parity of the final state is determined by the ground state of the capturing nucleus and the natural parity  $(-1)^l$  of the partial wave of the captured proton. Consequently, for s- and p-wave capture of a proton by <sup>27</sup>Al  $(J_0^{\pi} = 5/2^+)$ , levels with an angular momentum included in the spin ranges  $2^+$ ,  $3^+$  and  $1^-$ ,  $2^-$ ,  $3^-$ ,  $4^-$ , respectively, play a crucial role. Besides the intrinsic structure of the final state wave function, further requirements to enhance the capture rate are a considerable level/resonance width  $\Gamma$  of the capturing level and for excited states at least one sufficiently fast  $\gamma$ -ray decay to a bound state, which stabilises the newly formed nucleus against subsequent particle



<sup>&</sup>lt;sup>a</sup> e-mail: marcus.scheck@uws.ac.uk (corresponding author)

emission. In an even-even nucleus, low-spin states are usually connected to the ground state by  $\gamma$ -ray emission and, therefore, have the  $\gamma$ -ray decays with the highest possible transition energies  $E_{\gamma}$ ; the partial decay width  $\Gamma_{\gamma,f}$  to the final level f scales with  $E_{\gamma,f}^{2L+1}$ , where L is the multipolarity of the  $\gamma$ -ray transition with energy  $E_{\gamma,f}$ . Consequently, low-spin levels with ground-state transitions will have an enhanced  $\gamma$ -ray decay width  $\Gamma_{\gamma,f}$ , which means a comparably short lifetime  $\tau=\hbar/\Gamma$ . Consequently, these comparably wide doorway states with a significant  $\gamma$ -ray decay branch can be expected to play an important role in the astrophysical synthesis of elements.

In stellar environments, where the incident particles obey a Maxwell-Boltzmann distribution with relatively low energy on a nuclear scale, the capture level must be situated just above the separation threshold to enhance the reaction rate. For <sup>28</sup>Si the proton emission threshold is measured to be  $S_p = 11585.02(10)$  keV, the Q-value for  $\alpha$ -particle emission is  $Q_{\alpha} = -9984.14(1)$  keV, and the neutron threshold is  $S_n = 17179.72(14)$  keV [4]. However, in explosive scenarios, e. g. a type-1 supernova, the energy distribution of the incident particles contains high-energy particles and levels situated well above the threshold energy can act as doorways for the penetrating particle. Reference [5] provides a survey of the levels in <sup>28</sup>Si and their contribution. In this compilation it is evident that the lifetime/width information for  $J^{\pi} = 1^{-}$ states is missing. These considerations provide strong motivation to investigate low-spin states with a  $\gamma$ -ray link to the ground state.

This work is part of an ongoing campaign [6–9] using  $(\gamma, \gamma')$  photon-scattering experiments [10,11] to investigate photo-excited levels in light  $N \approx Z$  nuclei using state-ofthe-art detector technology. Photo-excitation implies that the investigated levels must necessarily have a  $\gamma$ -ray transition linking the excited state to the ground state. Due to the vanishingly small momentum  $p_{\gamma} = E_{\gamma}/c$  of the incident photon, the angular momentum transfer in these nuclear resonance fluorescence (NRF) experiments is limited to the photons 1  $\hbar$  intrinsic angular momentum and, far less likely, a second unit of  $\hbar$ . Consequently, real photon scattering is selective to low-spin excitations. The incident photon, which excites the nucleus, defines a quantisation axis for the subsequent decay  $\gamma$  ray and the associated angular distribution allows spin assignments to be made. The scattering cross section for a decay channel f is proportional to the ground-state decay width  $\Gamma_0$  of the excitation path and the decay branching ratio  $\Gamma_f/\Gamma$  for the decay to the final state f. Using the experimentally determined, or previously known, branching ratios the extracted total level width  $\Gamma$  allows the level lifetime  $\tau = \hbar/\Gamma$  and reduced transition strengths to be calculated. Given that the scattering process involves solely the electromagnetic interaction, these quantities are determined in a model-independent approach.

As outlined above, for even-even nuclei the inelastic scattering of real photons prefers the excitation of J = 1 states. Therefore, NRF [10,11] tests the E1 electric ( $J^{\pi} = 1^{-}$ ) [12] and M1 magnetic  $(J^{\pi} = 1^{+})$  [13] dipole responses of the investigated nucleus. The M1 response is dominated by isoscalar spin-flip excitations and the isovector Gamow-Teller resonances (GTR) [14,15]. The spin-isospin  $\vec{\sigma} \vec{\tau}$  GTR excitations, involving spin  $\vec{\sigma}$  and isospin  $\vec{\tau}$  degrees of freedom, determine the inelastic neutrino-scattering cross sections [16], which are important reactions for type-II corecollapse supernovae. A recent  ${}^{28}Si(p, p')$  295 MeV inelastic proton scattering experiment [17,18] disentangled these modes. The E1 distribution is dominated by the Giant Dipole Resonance (GDR) [14,15], which in <sup>28</sup>Si is situated near 20 MeV [19] and exhibits a pronounced fine structure [20]. In the investigated energy regime on the low-energy tail of the GDR, the E1 strength is addressed as Pygmy Dipole Resonance (PDR) [21–23]. The PDR is in a hydro-dynamical model visualised as an oscillation of a skin formed by excess neutrons versus an isospin saturated core, but also alternative mechanisms such as clustering or a toroidal mode [24-26] are proposed to contribute. For the N = Z nucleus <sup>28</sup>Si, it can be expected that the skin-mode is not present. Indeed previous  $(\gamma, \gamma')$  studies revealed only marginal E1 strengths for the N = Z nuclei <sup>24</sup>Mg [6] and <sup>40</sup>Ca [27]. Nevertheless, the presence of enhanced E1 strength in a  $N \approx Z$  nucleus would provide strong evidence that the nuclear E1 response is a shell effect caused solely as a result of particle-hole excitations across oscillator shell gaps of the type  $[(d_{5/2}^+)^{-1}, f_{7/2}^-]_{1}^$ or  $[(p_{1/2^-})^{-1}, d_{3/2^+}]_{1^-}$ . A recent study demonstrated for <sup>208</sup>Pb the role played by the underlying single-particle structure in the emergence of the PDR [28].

Experimental evidence for photo-excitable 1<sup>-</sup> levels in <sup>28</sup>Si was provided recently, when a  $(\vec{\gamma}, \gamma')$  experiment using fully-polarised, quasi-monochromatic  $\vec{\gamma}$  rays in the entrance channel reported such states for <sup>28</sup>Si [7]. This experiment confirmed also the proposed 1<sup>-</sup> nature [5] of a level at 10994 keV. However, to extract photon-scattering cross sections and related quantities like level lifetimes, decay widths, and reduced transition strengths requires knowledge of the absolute photon flux, a quantity that is notoriously difficult to determine for a quasi-monochromatic photon beam. For this task, NRF using unpolarised bremsstrahlung is favorable. In this approach the spectral distribution can, to a good degree be approximated using the Schiff formula [29] and the absolute flux can be determined by the use of a reference isotope with well-known scattering cross sections, e.g. <sup>11</sup>B [30–33]. Since the cross sections are determined relative to those for the reference isotope, various sources of systematic uncertainty are avoided. In particular, the knowledge of a relative  $\gamma$ -ray detection efficiency is sufficient. Interestingly, a previous  $(\gamma, \gamma')$  experiment [34] using partially polarised bremsstrahlung beams in the entrance channel reports the M1



strength to  $J^{\pi}=1^+$  levels but neglects the E1 strength to  $J^{\pi}=1^-$  levels. In addition, the aforementioned  $^{28}\mathrm{Si}(\alpha,\alpha')$  inelastic  $\alpha$ -particle scattering experiment [35] revealed several  $1^-$  states, for which no lifetime and, therefore, resonance width is known. It is the aim of this work to provide this additional piece of spectroscopic information and test whether the E1 strength of these levels is substantial.

Previous work characterised <sup>28</sup>Si as moderately oblate deformed in the ground state [36]. This statement is supported by the standard indicator for quadrupole deformation, namely the  $E_{4/2} = E_{4_1^+}/E_{2_1^+}$  ratio of the excitation energies of the first  $J^{\pi} = 4_1^+$  and first  $2_1^+$  levels. For <sup>28</sup>Si this value is  $\approx 2.6$  [4], which is well below the expected value for a welldeformed nucleus and rather in line with a  $\gamma$ -soft nucleus. Additionally, a prolate deformed structure built upon a 0<sup>+</sup> state at 6691 keV is proposed as well as a super-deformed structure with an underlying  $\alpha$ -cluster structure [37]. From a shell-model perspective, <sup>28</sup>Si is quite interesting. Both protons and neutrons have a fully filled  $1d_{5/2}$  subshell, with the  $2s_{1/2+}$  subshell near the Fermi surface. The presence of a  $s_{1/2^+}$  near the Fermi surface often causes a reduction of collective effects and the closed subshells resemble a doublymagic system. Furthermore, no intruder subshell that would allow for low-lying negative-parity excitations is present in the oscillator shell.

The  $^{24}$ Mg( $\gamma$ ,  $\gamma'$ ) study [6] exhibited branching ratios for the ground-state decay relative to the decay to the first excited  $2_1^+$  state that are in-line with the assignment of a K=1projection quantum number via the Alaga rules [38]. This observation together with the in photon scattering experiments [10,39] well-established applicability of these rules for well-deformed nuclei provides an evidence for the prolate deformed character of  $^{24}$ Mg. The  $^{28}$ Si( $\vec{\gamma}$ ,  $\gamma'$ ) study [7] observed, for two of the photoexcited states, branching transitions to lower-lying excited states. Moreover, the first excited  $0_2^+$  state at 4979.9 keV [4] exhibits a remarkable E0 strength of  $\rho(E0, 0_2^+ \to 0_1^+) \times 10^3 = 262(31)$  [40,41], indicating a strong mixing of the  $0_1^+$  ground state and the  $0_2^+$  state and possibly a large difference  $\Delta \beta_2^2$  of the two  $\beta_2$  deformation parameters [42,43]. Therefore, it is of interest to test whether an approach outlined in Ref. [44] and applied to <sup>24</sup>Mg [6], namely using the branching ratio of the observed  $J^{\pi} = 1^{+}$ states to these  $0^+$  states to extract the mixing parameters, results in a consistent picture. This would allow to extract the mixing of the two  $0^+$  levels and allow the relative shape differences [43] to be quantified.

## 2 Experiment

The experiments were conducted using the ELBE particle accelerator of the Helmholtz-Zentrum Dresden-Rossendorf,

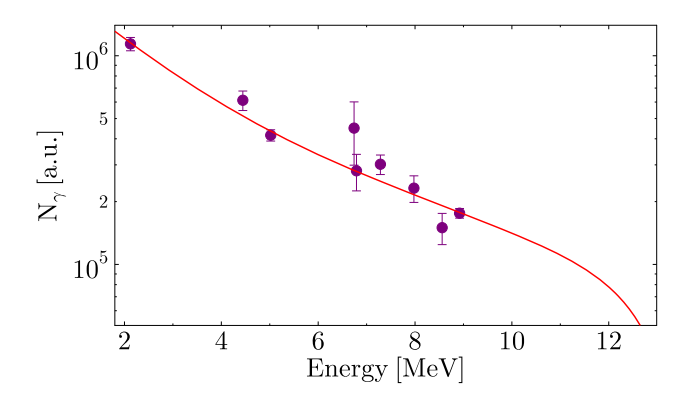


**Fig. 1** Photon-flux distribution  $N_{\gamma}(E_{\gamma})$  described by the Schiff formula [29]. The curve is obtained in an error-weighted fit to the experimental points of the well-known transitions of <sup>11</sup>B [30–33]. Note the logarithmic scale on the y axis

which provided 13.0 MeV electrons. Those bombarded a 12.5  $\mu$ m thin niobium target to produce unpolarised bremsstrahlung  $\gamma$  rays. Throughout the 122 h of the experiment a stable electron current of 287(2)  $\mu$ A was impinging on the radiator target.

The bremsstrahlung photons enter the  $\gamma$ ELBE cave via a circular hole in a 2.6 m thick aluminum collimator. In the cave the photons travel in an evacuated beam tube with a pressure of approximately  $10^{-5}$  mbar to minimise background due to scattering with air molecules [45]. Photons that do not react with the target are stopped approximately 4 m downstream in the beam dump.

The 4199.1(5) mg of silicon dioxide (SiO<sub>2</sub>) target material was pressed into a thin disc, which was rotated by approximately 45° relative to the incoming photon beam and the front planes of the detectors. This approch minimises the pathlength the photons travel through the target material and, therefore, reduces absorption. The silicon was enriched to >99.0 % in the A=28 isotope and sandwiched between two further discs, each made of 300.0(5) mg of enriched (99.5 %) <sup>11</sup>B. The well-known transitions from photo-excited levels of <sup>11</sup>B [30–33] serve as a photon-flux calibration standard. This relative measurement removes the need to determine absolute  $\gamma$ -ray detection efficiencies  $\epsilon_{abs}(E_{\gamma})$  and an absolute photon flux  $N_{\gamma,abs}(E_L)$ . The photon-flux distribution for a thin radiator target is described by the Schiff formula [29]. An error-weighted fit of this distribution to the experimental points of levels of <sup>11</sup>B is shown in Fig. 1. Typical uncertainties for the fit of the photon flux were  $\approx 2\%$ ; However, to account for systematic effects, such as a thicker radiator target or uncertainties with the photon-beam end point, an uncertainty was added. Within the energy range covered by the photo-excited levels of <sup>11</sup>B (4444 keV - 8920 keV) a relative uncertainty of 5 % and of 10 % outside this range were assumed for the photon flux.



186 Page 4 of 15 Eur. Phys. J. A (2025) 61:186

The target position is surrounded by four high-purity germanium detectors (HPGe) of the  $\gamma$ ELBE setup [46]. Two detectors were positioned at  $\theta = 90^{\circ}$  and two detectors at  $\theta = 127^{\circ}$  with respect to the momentum direction of the photon beam. All detectors have a  $\gamma$ -ray detection efficiency of approximately 100 % relative to the  $3'' \times 3''$  NaI calibration standard. The target to detector distance was approximately 28 cm for the 90° detectors and 32 cm for the 127° detectors. Each 90° detector covers an angular range of  $\Delta\theta=16^\circ$ and each 127° detector a range of  $\Delta\theta = 14^{\circ}$ . All detectors were equipped with an active anti-Compton shielding; however, for one of the 90° detectors, the active shielding failed. Of course, for this detector the peak-to-background ratio is noticably reduced, when compared to the Comptonsuppressed spectra. Nevertheless, the missing suppression in one detector allows in comparison to spectra recorded in suppressed detectors a quick and firm identification of singleand double-escape peaks. The spectra were recorded in singles mode. Therefore, the pre-amplifier signals were directly fed into LYNX digitizers and recorded in anti-coincidence with the signals from the active anti-Compton shield. Attenuators were placed between target and detector to prevent undesired low-energy photons from reaching the detectors. This limits the counting rate to below 15 kHz and reduces the pile-up probability. For the two 90° detectors, the attenuators had thicknesses of 8 mm of natural lead and 3 mm of copper, while for the 127° detectors the attenuators consisted of 3 mm of lead and 3 mm of copper. The relative  $\gamma$ -ray detection efficiency was simulated using the GEANT software package [47]. These simulated efficiencies were tested using a variety of reactions, details can be found in Ref. [48]. In order to analyse spectra with the maximum available statistics, the spectra recorded in the two detectors positioned at the same angle were added. A spectrum created by adding the two spectra recorded in the detectors positioned at  $\theta = 127^{\circ}$  is shown in Fig. 2. Below photon energies of about 5 MeV, background due to Compton scattering off the atomic systems is present. Above 5 MeV the spectrum shows the excellent background conditions for NRF experiments at  $\gamma$ ELBE, which enable the identification even of low-intensity transitions.

In NRF experiments, the incoming photon beam provides a quantisation axis relative to which the resonantly scattered photons exhibit pronounced angular distributions  $W(\theta)$ . For unpolarised bremstrahlung,  $W(\theta)$  solely depends on the polar angle  $\theta$ , that is defined by the directions of the absorbed and emitted photons. The  $J^{\pi}=0^+$  ground state of even-even nuclei, like <sup>28</sup>Si, and the low momentum transfer in real photon scattering results in the spin-selectivity to J=1 levels and, to a lesser extent,  $2^+$  states. For resonant scattering with excitation from and decay to the ground state involving an intermediate level with one of these spins, the angular distributions exhibit the most pronounced ratios  $W(\theta_1)/W(\theta_2)$  for the scattering angles  $\theta_1=90^\circ$  and  $\theta_2=127^\circ$ . Hence the

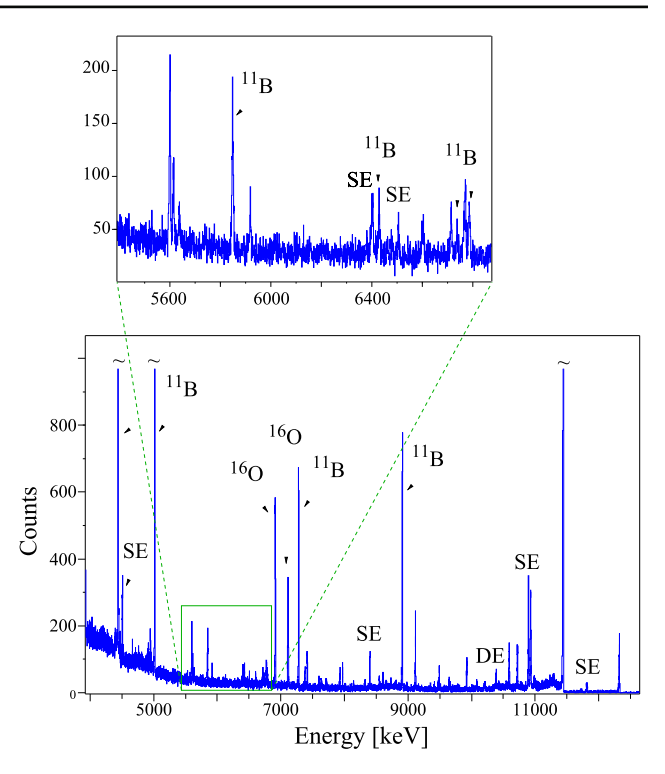


Fig. 2 Bottom:  $\gamma$ -ray spectrum resulting from the addition of the spectra recorded in the two HPGe detectors positioned at  $\theta=127^\circ$ . Peaks associated with the photon-flux calibration standard boron-11 are marked with  $^{11}$ B, transitions identified to belong to oxygen-16 as  $^{16}$ O, and single/double-escape peaks, which are still present in suppressed spectra, are marked with SE/DE. In order to emphasize low-intensity transitions, the y-axis was limited to approximately 1000 counts per channel. More intense transitions that are not fully shown are indicated using a tilde above. The top shows a section of the spectrum with comparably low-intensity transitions

detectors were positioned at these angles. For a J=1 level as an intermediate state, a ratio of 0.707 is expected and for a J=2 level a ratio of 2.2. Further values for angular distributions  $W(\theta)$  for various possible cascades and the ratios for the two angles realised in the experiment are presented in Table 1 of Ref. [6]. In terms of experimental quantities, the ratio  $R_{90/127}$  is defined by

$$R_{90/127} = \frac{W(90^{\circ})}{W(127^{\circ})} = f_{90/127} \frac{\frac{A(90^{\circ})}{\epsilon(90^{\circ}, E_{\gamma})}}{\frac{A(127^{\circ})}{\epsilon(127^{\circ}, E_{\gamma})}}.$$
 (1)

Here,  $A(\theta)$  is the peak area in the spectrum recorded in the detector positioned at the angle  $\theta$ ,  $\epsilon(\theta, E_{\gamma})$  is the relative full-energy detection efficiency of the detector at the angle  $\theta$  for the  $\gamma$ -ray energy  $E_{\gamma}$ , and  $f_{90/127}$  is a cross-normalisation factor that is fixed by a source calibration and tested using the transitions of the photon-flux calibration standard,  $^{11}$ B. Additionally, two excitations in  $^{16}$ O, included in the SiO<sub>2</sub> target material, allowed a verification for the target material itself. Furthermore, the detectors at  $90^{\circ}$  receive an enhanced



Eur. Phys. J. A (2025) 61:186 Page 5 of 15 186

rate of Compton-scattered events compared to the detectors at 127°, which results in higher count rates and, consequently, higher dead time of the electronics. However, the source and <sup>16</sup>O in-beam verifications assure that no pronounced dead-time effects influence the quality of the extracted data.

The energy-integrated photon scattering cross section,  $I_{S,f}$ , for a  $\gamma$ -ray transition to the final level, f, is related to experimental quantities by

$$I_{S,f} \propto \frac{1}{n_T} \frac{A}{\epsilon(E_{\gamma}) \cdot N_{\gamma}(E_L) \cdot W(\theta)},$$
 (2)

namely, the number of target nuclei  $n_T$ , the peak area A, the angular distribution function  $W(\theta)$ , the relative  $\gamma$ -ray detection efficiency  $\epsilon(E_\gamma)$ , and the relative photon flux  $N_\gamma(E_L)$  at the energy of the photo-excited level  $E_L$ . For the angular distribution, the calculated values as given in Table 1 of Ref. [6], are used for the cascades indicated in Column 6 of Table 1 in this work. Henceforth, energy integrated indicates that the cross section is integrated over the energy range of the resonance width  $\Gamma = \sum_f \Gamma_f$ , corresponding to the sum over the partial decay widths  $\Gamma_f$  for the f decay channels. In NRF the energy-integrated scattering cross section  $I_{S,f}$  is linked to the resonance widths via

$$I_{S,f} = \pi^2 \left(\frac{\hbar c}{E_L}\right)^2 g \Gamma_0 \frac{\Gamma_f}{\Gamma},\tag{3}$$

where  $E_L$  is the level energy,  $g=(2J_L+1)/(2J_0+1)$  is a statistical factor including the level spin  $J_L$  and the ground-state spin  $J_0$ ,  $\Gamma_0$  the ground-state width of the excitation path, and  $\Gamma_f/\Gamma$  the branching ratio of the partial decay width  $\Gamma_f$  and total decay width  $\Gamma$  for the decay path. Considering that the partial decay width  $\Gamma_f \propto I_{S,f}$  scales with the energy-integrated scattering cross section, the total level width  $\Gamma$  can be obtained. Furthermore, the relation  $\tau=\hbar/\Gamma$ , allows the determination of the level lifetime and, subsequently, the reduced transition probabilities  $B(\Pi L, J_i \rightarrow J_f)$  can be calculated.

The assignment of a K quantum number via the theoretical values calculated with the Alaga rules [38] is discussed in detail in Refs. [6,10,39]. The Alaga rules are valid for well-deformed nuclei, for which the  $0_{gs}^+$  ground state is the bandhead of a rotational band that includes the  $2_1^+$  state as first excited level. The experimental ratio  $R_{Al,exp}$  is compared to theoretical values  $R_{Al,theo} = 2$  for K = 0 and  $R_{Al,theo} = 0.5$  for K = 1, which are calculated as ratios of two Clebsch-Gordan coefficients. The experimental value

$$R_{Al,exp} = \frac{I_{S,2_1^+}}{I_{S,0_1^+}} \cdot \frac{E_{\gamma,0_1^+}^{2L+1}}{E_{\gamma,2_1^+}^{2L+1}}$$
(4)

involves the scattering cross sections  $I_{S,f}$  for the two decays from the photo-excited  $J^{\pi}=1^{\pi}$  level to the first excited  $2_1^+$  level and the  $0_1^+$  ground state, the energies  $E_{\gamma,f}$  of the two connecting  $\gamma$ -ray transitions, and the transition multipolarity  $I_{\gamma}$ .

#### 3 Results

The excellent background conditions at the  $\gamma$ ELBE setup allowed the first identification of several weaker transitions. Some of these transitions were on the verge to be background fluctuations. In this work, for a peak to be counted as such, the following criteria were applied. If the average background exceeded 20 counts per channel, a Gaussian distribution of the background counts is assumed and the peak area is expected to exceed three standard deviations of the number of background counts underneath the peak. For an average background between 10 and 20 counts per channel, which is transitional between Poisson and Gaussian distributed background, a minimum peak area of four standard deviations is demanded, and if the average background is below 10 counts per channel a Poisson distribution is valid and five standard deviations are demanded. The energies of the observed  $\gamma$ -ray transitions were corrected for recoil effects and are presented in Table 1. Uncertainties of the  $\gamma$ -ray energies contain the fitting error and systematic uncertainty associated with the energy calibration. To account for the uncertainty of the calibration, below 8917 keV, which is the highest-lying observed  $\gamma$  ray associated with <sup>11</sup>B, an uncertainty of  $\Delta E_{\gamma} = 0.3 \text{ keV}$ was added and, above this energy, 0.5 keV. If multiple transitions were observed to depopulate a level, the level energy was calculated using an error-weighted average of the recoilcorrected  $\gamma$ -ray energy. The assignment of observed  $\gamma$ -ray transitions to levels followed the literature [4]. All newly observed transitions were assigned to known levels using the Rydberg-Ritz variation principle by checking whether the sum of energies of the known low-lying level and the newly observed  $\gamma$ -ray transition match the energy of a previously known level. Furthermore, the energy difference between the two newly observed transitions at 12330.7(10) keV and 10550.4(12) keV matches the energy of the first  $2_1^+$  level. Hence, these transitions are assigned to depopulate a level at 12330.2(8) keV to the ground-state and first excited 2<sup>+</sup> state, respectively. Newly observed transitions are indicated in Table 1.

Additionally to the desired transitions from <sup>28</sup>Si, transitions associated with the photon-flux calibration standard <sup>11</sup>B were identified as well as transitions associated with <sup>16</sup>O. Of course, scattering off oxygen from other parts of the setup cannot be excluded. Nevertheless, due to the considerable amount of oxygen in the target, it still can be safely assumed that in-target scattering dominates. Hence, the well-known



186 Page 6 of 15 Eur. Phys. J. A (2025) 61:186

properties of the 6917-keV and 7116-keV levels of <sup>16</sup>O [49] served as a check for the analysis. As shown in Fig. 3, for both transitions the angular distribution ratio agrees with the expected values. For transitions associated with <sup>28</sup>Si, the  $W(90^{\circ})/W(127^{\circ})$  ratios confirm for the levels with the most intense transitions the accepted spin assignments [4,7] and in the case of the 12330-keV level allow an assignment of J = 1. However, for the majority of observed transitions, the level of statistics is too low and the associated uncertainty does not allow any conclusions to be made. For decay transitions that possibly are of mixed multipolarity, the level of statistics is not sufficient to narrow down the range for the multipole-mixing ratio. In order to provide the opportunity to correct for a possibly wrongly assumed multipolarity and the associated angular distribution, the combination of transition multipolarities used to calculate the integrated scattering cross section  $I_{S,f}$  (see Eq. 2) is given in Column 6 of Table 1. Interestingly, even if no feeding transition is observed, a less pronounced angular distribution provides an indication for unseen feeding into the depopulated level. The fractions for the population via photo-excitation and feeding (isotropic angular distribution) were extracted by adjusting the weighting of the two angular distribution values until the energyintegrated scattering cross sections for both detectors were identical. However, given the often low statistics, these values should be treated with utmost care and rather provide a rough guidance. Anyway, as elucidated later, the integrated scattering cross sections for these transitions represent just upper limits as do the quantities calculated from these cross sections. Another strong indication for feeding into a level is the extracted level lifetime. Feeding enhances the depopulation of a given level and the energy-integrated cross section appears too high. Consequently, the extracted decay width is too wide and the resulting lifetime too short when compared to the known values from the literature. In Table 5 the lifetimes extracted in this work are compared to the available literature values [4]. Indeed, with the exception of the 9479-keV state and eventually the 9495-keV state, all levels up to 9795 keV exhibit indications for feeding and the given lifetimes must be regarded as (robust) lower limits.

The extracted energy-integrated scattering cross sections and subsequently extracted decay widths and reduced transition strengths are presented in Tables 2 and 3. These tables contain for each level the observed transitions and their extracted energy-integrated scattering cross section  $I_{S,f}$ , calculated partial decay width  $\Gamma_f$ , the total decay width  $\Gamma$ , and the reduced transition probability  $B(\Pi L) \downarrow$ . Table 2 includes the levels with a firmly assigned as well as those of suspected positive parity and Table 3 contains the levels with a firmly assigned spin and parity combination of  $J^{\pi} = 1^-$ . In the case of levels, where further decay transitions are known in the literature, and which were not seen in the experiment, their relative intensities were used in the calculation of the partial

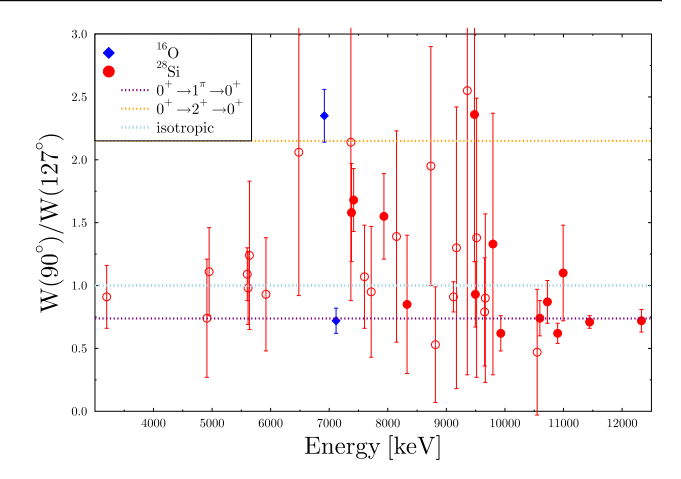


**Fig. 3** Ratio  $W(90^\circ)/W(127^\circ)$  of the angular distribution function at the two angles  $\theta = 90^\circ$  and  $\theta = 127^\circ$ , where the detectors were positioned. In addition to the transitions attributed to <sup>28</sup>Si, ratios of two transitions from <sup>16</sup>O are shown. Full circles indicate transitions that connect a level in <sup>28</sup>Si to the ground state and open circles represent transitions that end in a lower-lying excited state

decay width  $\Gamma_f$  and total decay width  $\Gamma$ . The levels for which this additional information is considered are indicated by a footnote. The extracted quantities are obscured if a level is affected by the aforementioned feeding. For the lower-lying levels, which receive feeding, there are two scenarios. First, the level was exclusively populated by feeding. These levels are not included in Table 2. Second, if a level was populated by photon scattering from the ground state as well as feeding, the  $I_{S,f}$  is given as an upper limit, that is in Table 2 the sum of the calculated value plus the uncertainty. The set of measured  $I_{S,f}$  values was used to calculate the partial decay widths  $\Gamma_f$ for the observed  $\gamma$  rays and, subsequently, the level lifetime  $\tau$  and reduced transition probabilities  $B(\Pi L) \downarrow$  between the photo-excited level and the lower-lying final states. For none of the transitions connecting two positive parity levels is an E2/M1 multipole-mixing ratio,  $\delta$ , known. Consequently, for all those transitions that do not allow only for an exclusive M1 multipolarity, the two possible reduced transition probabilities  $B(\Pi L) \downarrow$  are calculated as pure transitions and presented as upper limits. For these limits, the calculated values are presented with the uncertainties given separately.

Interestingly, for several levels a decay to a lower-lying excited state was observed, but no decay to the ground state. In NRF, which exclusively populates levels from the ground state, such a behaviour is unusual. For example, for the 10514-keV level the transition to the first excited level is known [4] to decay with a relative intensity of 100(2), while the ground-state decay intensity is given as 51(2). While the 8735-keV transition fulfills the criteria to be a peak, there were in neither of the two spectra significant peaks at the position of the ground-state transition. This observation can be explained by a combination of a lower relative  $\gamma$ -ray intensition.



Eur. Phys. J. A (2025) 61:186 Page 7 of 15 186

sity and a lower  $\gamma$ -ray detection efficiency at the higher  $\gamma$ -ray energy. If in the literature [4] the intensity of the groundstate transition is known, this branching ratio was used to calculate the transition widths and reduced transition rates. However, some  $\gamma$ -rays are observed that, using the Rydberg-Ritz's variation principle, do connect known levels, but no ground-state decay of the upper level is known. These  $\gamma$ ray transitions are given in Table 4 together with the levels to which they are attributed. The comparatively high excitation of all these levels renders a population due to unseen feeding unlikely. Supporting the conclusion that these levels have a ground-state branch is the circumstance that they all have been excited in the (p, p') inelastic proton scattering reaction [50]. For the case that a future experiment determines the ground-state branching ratio, Table 4 provides the energy-integrated scattering cross section so the subsequent quantities can be calculated.

The extracted half-lives are shown in Table 5. Apart from the 9479-keV level, all levels below 9.5 MeV are subject to feeding and their extracted half-lives can only be considered as lower limits. Interestingly, the half-lives for the

**Table 1** Given are the energy,  $E_i$ , and spin-parity combination,  $J_i^{\pi}$ , of the initial level, the recoil-corrected  $\gamma$ -ray energy,  $E_{\gamma}$ , and the spin and parity  $J_f^{\pi}$  of the final level. Apart from the level at 12330 keV, for which this work allows an assignment of J=1, all spins and parities are taken from Refs. [4,7]. Column five presents the measured ratio  $W(90^{\circ})/W(127^{\circ})$  of the angular distributions at  $\theta=90^{\circ}$  and  $\theta=127^{\circ}$ .

two strongest excited levels at 10900 keV and 11446 keV determined in this work are approximately 10-20% larger when compared to the literature values. Indeed, when compared with the previous  $(\gamma, \gamma')$  measurement [34], the values agree within the uncertainties but the present lifetime values are slightly longer. However, since Berg et al. neither elucidate their method to calibrate the photon flux nor how the response of their detectors was determined, any attempt to resolve this discrepancy is pure speculation. Compared to the (p, p') and (e, e') particle-scattering experiments, a possible reason for longer lifetimes in the present work is that it misses the  $\alpha$ -particle decay channel, while particle scattering experiments are insensitve to the way the excited level depopulates. However, for  $J^{\pi} = 1^{+}$  the positive parity renders the  $\alpha$  decay unlikely. This is supported by data from the  $^{24}$ Mg( $\alpha$ ,  $\gamma$ ) reaction, which populates the 10514-keV  $2^+$ , the 10995-keV 1<sup>-</sup>, and 11295-keV 1<sup>-</sup> natural parity levels [51– 54], but no  $J^{\pi} = 1^+$  levels. Unfortunately, for none of these three levels a lifetime was known, so that the comparison of newly obtained and previously known widths would have allowed an extraction of the  $\alpha$ -decay width  $\Gamma_{\alpha}$ . Furthermore,

If no  $W(90^\circ)/W(127^\circ)$  ratio is given, the  $\gamma$  ray was observed only in one detector. Column 6 provides the multipolarities  $\Pi_1L_1-\Pi_2L_2$  as used in the calculation of the energy-integrated scattering cross section. If Column 6 is empty, it is assumed that the level population happened exclusively by feeding from higher-lying levels

$E_i$ [keV]	$J_i^\pi$	$E_{\gamma}$ [keV]	$J_f^\pi$	W(90°)/W(127°)	$\Pi_1L_1$ - $\Pi_2L_2$
1779.2(4)	2+	1779.2(4)	0+	1.21(11)	30 % E2-E2 + 70 % isotropic
4618.4(6)	4 <sup>+</sup>	2839.4(5)	2+	0.65(41)	
4980.2(6)	0+	3201.2(5)	2+	0.91(25)	
6691.2(9)	0+	4912.2(8)	2+	0.74(47)	
7380.5(4)	2+	7380.7(7)	$0_{+}$	1.58(39)	40 % E2-E2 + 60 % isotropic
		5601.4(5)	2+	1.09(21)	40% <i>E</i> 2- <i>E</i> 2 + 60 % isotropic
7417.4(6)	2+	$7416.9(9)^a$	0+	1.68(25)	20% E2-E2 + 80% isotropic
		5638.8(8)	2+	1.24(59)	20% E2-E2 + 80% isotropic
7933.5(6)	2+	7933.5(6)	$0_{+}$	1.55(34)	65% E2-E2 + 35% isotropic
8259.6(11)	2+	6480.6(10)	2+	2.1(12)	E2-E2
8328.4(9)	1+	8328.8(1)	$0_{+}$	0.85(55)	M1-M1
		$6547.8(21)^a$	2+		M1-M1
9381.3(9)	2+	7602.3(8)	2+	1.07(41)	50% E2-E2 + 50% isotropic
9479.1(11)	2+	9479.1(11)	0+	2.4(12)	E2-E2
9495.9(6)	1+	9495.7(8)	0+	0.93(26)	M1-M1
		7717.3(10)	2+	0.95(52)	M1-M1
9795.3(12)	$(2^{+})$	9793.9(18)	0+	1.3(11)	E2-E2
		8017.2(15)	2+	0.45(68)	E2-M1
9929.5(4)	1-	9929.7(7)	0+	0.62(14)	E1-E1
		8149.7(12) <sup>c</sup>	2+	1.39(84)	E1-E1
		4949.6(5) <sup>c</sup>	0+	1.11(35)	E1-E1



186 Page 8 of 15 Eur. Phys. J. A (2025) 61:186

m 11 1	
Table 1	continued

$E_i$ [keV]	$J_i^\pi$	$E_{\gamma}$ [keV]	$J_f^\pi$	W(90°)/W(127°)	$\Pi_1L_1$ - $\Pi_2L_2$
10514.4(13)	(2 <sup>+</sup> )	8735.4(12)	2+	1.95(95)	E2-E2
10595.3(5)	1+	10596.7(12)	$0_{+}$	0.74(14)	M1-M1
		8813.7(13) <sup>c</sup>	2+	0.53(46)	M1-M1
		5615.6(6)	$0_{+}$	0.98(29)	M1-M1
10725.1(8)	1+	10725.1(8)	$0_{+}$	0.87(17)	M1-M1
10900.1(5)	1+	10900.4(11)	$0_{+}$	0.62(8)	M1-M1
		9121.2(12)	2+	0.91(12)	M1-M1
		5919.8(7) <sup>c</sup>	$0_{+}$	0.93(45)	M1-M1
		$3484.5(11)^{b,c}$	2+		M1-M1
10951.3(2.2)	$(1, 2^+)$	9172.3(21)	$2^+$	1.3(11)	E2-E2
10993.8(13)	1-	10993.6(15) <sup>c</sup>	0+	1.10(38)	E1-E1
		$9215.2(25)^b$	2+		E1-E1
$11136.8(24)^d$	$(2^{+})$	9357.8(23)	2+	2.6(23)	E2-E2
11295.9(14)	1-	11296.4(13) <sup>e</sup>	0+	0.55(48)	E1-E1
		9516.4	2+	1.4(11)	E1-E1
11432.6(10)	$(2^{+})$	9653.6(9)	2+	0.79(43)	E2-M1
11445.7(7)	1+	11446.2(8)	$0_{+}$	0.71(5)	M1-M1
		9665.5(12) <sup>c</sup>	2+	0.90(67)	M1-M1
11987.0(13)	2+	$10203^{f}$	2+		
		7369.1(12) <sup>c</sup>	4+	2.1(13)	E2-E2
12330.2(8)	1(+)	12330.7(10) <sup>c</sup>	0+	0.72(9)	M1-M1
		$10550.4(12)^{c}$	2+	0.47(50)	M1-M1

<sup>&</sup>lt;sup>a</sup>Seen only in  $\theta = 90^{\circ}$  detector

the 12330-keV level is the only photo-excited state which is positioned above the proton-emission threshold. Indeed, this level was observed in the  $(p,\gamma)$  reaction [51], but again no lifetime was known prior to this work. Once the proton to  $\gamma$ -ray branching ratio is measured, the integrated scattering cross sections presented in Table 2 will allow a calculation of the lifetime. The present value was determined assuming  $\Gamma_p=0$  and represents realistically rather an upper limit for the half-life.

# 4 Discussion

The aim of this work was to provide information about the  $J^{\pi}=1^-$  states and to test the results for  $J^{\pi}=1^+$  levels [34]. The extracted E1 strength distribution of  $^{28}$ Si is shown in Fig. 4, where it is compared to the strength distributions of the other N=Z nucleus  $^{24}$ Mg [6] and the N=Z+2 nucleus  $^{26}$ Mg [8]. These nuclei are compared, because they

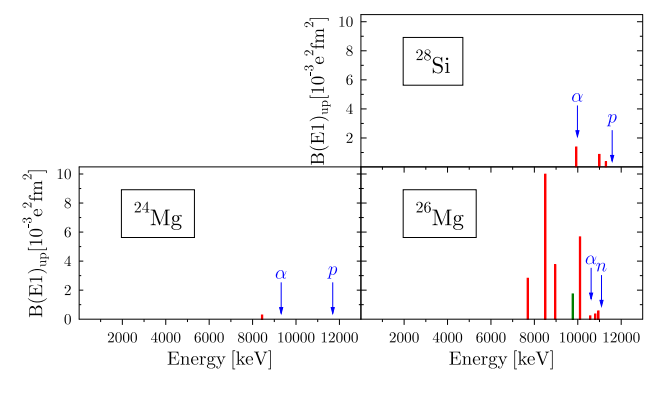


Fig. 4 Systematics of the  $B(E1,0^+_{gs}\to 1^-)$  excitation strengths for the nuclei  $^{24}$ Mg [6],  $^{26}$ Mg [8,9], and  $^{28}$ Si. The plot is arranged according to the relative position of the nuclei in the Segre chart. E1 strength to a level with firmly assigned  $J^\pi=1^-$  is presented as red bar and E1 strength to a level with tentative negative-parity assignment  $J^\pi=1^{(-)}$  is shown as green bar. Furthermore, the relevant emission thresholds for the emission of  $\alpha$  particles  $(\alpha)$ , protons (p), and neutrons (n) are indicated



<sup>&</sup>lt;sup>b</sup>Seen only in  $\theta = 127^{\circ}$  detector

<sup>&</sup>lt;sup>c</sup>Transition not in Ref. [4]

<sup>&</sup>lt;sup>d</sup> Assuming level to correspond to 11142-keV level in Ref. [4]

<sup>&</sup>lt;sup>e</sup>Peak on Compton edge of intense 11445-keV peak

f Peak covered by single-escape peak

Eur. Phys. J. A (2025) 61:186 Page 9 of 15 186

**Table 2** Data of levels with an assigned positive parity, for which at least limits for the decay width  $\Gamma_f$  and reduced transition probabilities  $B(\Pi, L) \downarrow$  can be calculated. Given are the energy of the initial level,  $E_i$ , and its spin and parity,  $J_i^{\pi}$ , the  $\gamma$ -ray energy,  $E_{\gamma}$ , of the observed transition, the spin and parity,  $J_f^{\pi}$ , of the final level, the measured energy-integrated cross section,  $I_{s,f}$ , the calculated partial decay width,  $\Gamma_f$ , the total decay width,  $\Gamma_{tot}$ , and the calculated reduced transitions.

sition probabilities  $B(M1) \downarrow$  and  $B(E2) \downarrow$ . For levels that are fed by higher-lying levels,  $I_{S,f}$  is given only as an upper limit, which contains the value plus uncertainty. If a parity-conserving transition allows both multipolarities, the two possible reduced transition probabilities are given as upper limits. Please note for E2 transitions: 1 W. u. =  $5.05 \, \mathrm{e}^2 \mathrm{fm}^4$ 

E <sub>i</sub> [keV]	$J_i^\pi$	$E_{\gamma}$ [keV]	$J_f^\pi$	$I_{S,f}$ [eV·b]	$\Gamma_f$ [meV]	$\Gamma_{tot}$ [meV]	$B(M1) \downarrow [\mu_N^2]$	$B(E2) \downarrow \\ [e^2 fm^4]$
1779.2(4)	2+	1779.2(4)	0+	< 42	< 7	< 7		< 478
7380.5(4)	2+	7380.7(7)	$0^{+}$	< 10.4	< 94	$< 262^{a}$		< 5.3
		5601.4(5)	2+	< 18.4	< 169		< 0.080	< 39
7417.4(6)	2+	7416.9(9)	$0^+$	< 24.7	< 84	< 98		< 5.0
		5638.8(8)	2+	< 4.3	< 14		< 0.005	< 3.4
7933.5(6)	2+	7933.6(6)	$0^+$	< 16.8	< 55	< 68 <sup>a</sup>	< 2.2	
8259.6(11)	2+		0+	$< 0.5^{a}$	< 16	$< 175^{a}$		< 0.5
		6480.6(1)	2+	< 4.9	< 124		< 0.048	< 20
8328.4(9)	1+	8328.8(10)	0+	4.1(9)	55(27)	$< 260^{a}$	< 0.013	
		6547.8(21)	2+	5.1(22)	69(33)		< 0.036	< 16
9381.3(9)	2+		0+	$< 0.3^{a}$	< 41	< 1313		< 0.7
		$7602.3(8)^b$	2+	< 8.6	< 1167		< 0.26	< 69
9479.1(11)	2+	9479.1(11)	0+	12(3)	55(10)	$64(14)^a$		0.9(2)
9495.9(6)	1+	9495.7(8)	$0^{+}$	< 31	< 296	< 355	< 0.029	
		7717.3(10)	2+	< 7	< 59		< 0.012	< 3
9795.3(12)	2+	9793.9(18)	0+	< 7.2	< 58	< 88 <sup>a</sup>		< 0.9
		8017.2(15)	2+	< 3.3	< 27		< 0.005	< 1.1
10514.4(13)	$(2^{+})$		0+		$61(31)^a$	194(60) <sup>a</sup>		0.6(2)
		8735.4(12)	2+	7(2)	119(24)		$\leq 0.017(6)$	$\leq 3.1(14)$
10595.3(5)	1+	10596.7(12)	0+	78(7)	969(115)	1357(146) <sup>a</sup>	0.070(10)	
		8813.7(13)	2+	6(2)	73(10)		$\leq 0.012(2)$	$\leq 2.2(8)$
		5615.6(6)	0+	15(2)	188(23)		0.101(15)	
10725.1(8)	1+	10725.1(8)	$0^{+}$	72(6)	714(58)	714(58)	0.050(4)	
10900.1(5)	1+	10900.4(11)	0+	184(12)	2981(322)	4694(507)	0.199(20)	
		9121.2(12)	2+	91(6)	1473(160)		$\leq 0.168(17)$	$\leq 29(5)$
		5919.8(7)	$0^{+}$	8(2)	136(15)		0.057(6)	
		3485.5(11)	2+	6(2)	104(12)		$\leq 0.212(22)$	≤ 250(92)
11432.6(10)	$(2^{+})$		$0^{+}$		$141(29)^a$	1577(177) <sup>a</sup>		0.9(1)
		9653.6(9)	2+	17(4)	729(148)		$\leq 0.127(13)$	≤ 20(7)
11445.7(7)	1+	11446.2(8)	$0^{+}$	1838(81)	21030(952)	21170(960)	1.21(11)	
		9665.5(12)	2+	12(3)	140(37)		$\leq 0.013(4)$	≤ 2.1(6)
12330.2(8)	1(+)	12330.7(10)	$0^+$	251(16)	3514(894)	3725(947)	0.162(33)	
		10550.4(12)	2+	15(4)	211(54)		≤ 0.016(4)	$\leq 2.0(9)$

<sup>&</sup>lt;sup>a</sup> Value calculated using branching ratio taken from Ref. [4]

have been measured at the  $\gamma$  ELBE setup with similar photonflux endpoint energies and, consequently, comparable sensitivity. The observed low-lying E1 strength of <sup>28</sup>Si below 13 MeV exhausts only 0.026(2)% of the energy-weighted sum rule [27,55]

$$S(E1)_{EW} = \frac{9}{4\pi} \frac{\hbar^2 e^2}{2M} \frac{N \cdot Z}{A} = 14.8 \frac{N \cdot Z}{A} MeV \cdot e^2 fm^2.$$
 (5)

This value is an order of magnitude lower than the 0.23(5)% observed in the N = Z + 2 nucleus  $^{26}$ Mg, but in-line with the



<sup>&</sup>lt;sup>b</sup>Peak eventually contaminated by a transition from <sup>208</sup>Pb

186 Page 10 of 15 Eur. Phys. J. A (2025) 61:186

**Table 3** Data of levels with firmly assigned spin and parity of  $J^{\pi} = 1^{-}$  [7]. The table contains the energy of the initial level,  $E_i$ , the spin and parity,  $J^{\pi} = 1^{-}$ , of the photo-excited level, the  $\gamma$ -ray energy,  $E_{\gamma}$ , the

spin and parity,  $I_f^{\pi}$ , of the final level, the measured energy-integrated cross section,  $I_{S,f}$ , the partial decay width,  $\Gamma_f$ , the total decay width,  $\Gamma_{tot}$ , and the calculated  $B(E1) \downarrow$  reduced transition probability

$E_i$ [keV]	$J_i^\pi$	$E_{\gamma}$ [keV]	$J_f^\pi$	$I_{S,f}$ [eV·b]	$\Gamma_f$ [meV]	$\Gamma_{tot}$ [meV]	$B(E1) \downarrow$ $[10^{-3} e^2 \text{fm}^2]$
9929.5(4)	1-	9929.7(7)	0+	36(4)	471(80)	725(122)	0.46(11)
		8149.7(12)	$2^+$	4(1)	55(10)		0.13(5)
		4949.6(5)	0+	15(2)	199(34)		1.57(42)
10993.8(13)	1-	10993.6(15)	$0_{+}$	35(5)	403(66)	440(73)	0.29(8)
		9215.2(25)	2+	3.2(13)	37(7)		0.04(2)
11295.9(12)	1-	11296.4(13) <sup>a</sup>	$0_{+}$	9(3)	160(67)	247(104)	0.11(6)
		9516.4(14)	2+	5(2)	87(37)		0.10(5)

<sup>&</sup>lt;sup>a</sup>Peak on Compton-edge of intense 11446.2(8)-keV transition

**Table 4** Data of levels, for which neither a ground-state decay has been observed, nor is it known in the literature [4]. Given is the level energy,  $E_i$ , the spin and parity of the level,  $J_i^{\pi}$ , as found in the literature, the

observed  $\gamma$ -ray energy,  $E_{\gamma}$ , the spin and parity,  $J_f^{\pi}$ , of the final level, and the calculated integrated scattering cross section,  $I_{S,f}$ , for the observed  $\gamma$ -ray transition

E <sub>i</sub> [keV]	$J_i^\pi$	$E_{\gamma}$ [keV]	$J_f^\pi$	$I_{S,f}$ [eV·b]
10951.3(22)	$(1, 2^+)$	9172.3(21)	2+	3.5(11)
11136.8(24)	2+	9357.8(23)	$2^{+}$	3.6(12)
11987.0(13)	$2^+$	7369.1(12)	4+	7(2)

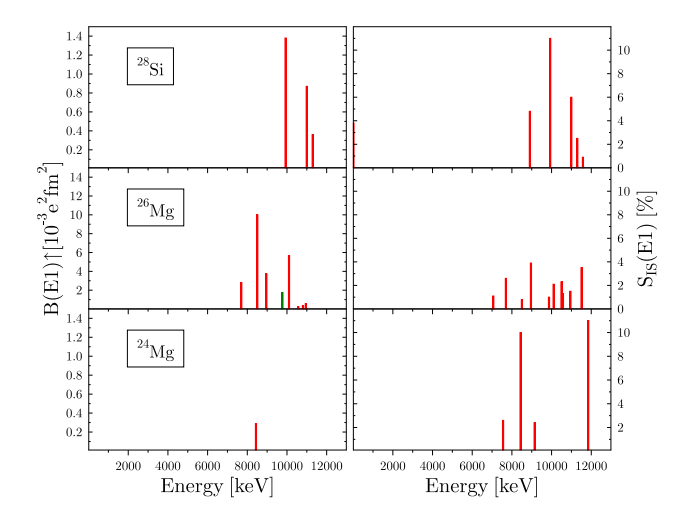


**Fig. 5** Comparison of the  $B(E1,0^+_{gs}\to 1^-)$  excitation strength extracted from  $(\gamma,\gamma')$  photon scattering (left side) and the fraction  $S_{IS}(E1)$  of the isoscalar energy-weighted sum rule as extracted from  $(\alpha,\alpha')$  inelastic  $\alpha$ -particle scattering [35] (right side). For an improved comparability the scale of the y-axis for the  $^{26}{\rm Mg}(\gamma,\gamma')$  results is adjusted

other N = Z nuclei in the investigated mass region [6,27] and experimentally confirms the negligible E1 strength in N = Z nuclei.

Conclusions about the isoscalar or isovector character of the observed  $1^-$  states can be drawn when comparing the pattern of the E1 excitation strength with that obtained in inelas-

tic scattering of the isoscalar  $\alpha$  particle [56–58]. Such a comparison of the  $B(E1, 0_{gs}^+ \rightarrow 1^-)$  excitation strength obtained in NRF with the fraction  $S_{IS}(E1)$  of the isoscalar energyweighted sum rule from an  $(\alpha, \alpha')$  inelastic  $\alpha$ -particle scattering experiment using the K600 spectrograph at iThemba Labs [35] is shown in Fig. 5. For all three nuclei <sup>24</sup>Mg,  $^{26}$ Mg, and  $^{28}$ Si, the  $(\alpha, \alpha')$  reaction revealed more potential  $J^{\pi} = 1^{-}$  levels, especially towards higher energies where the NRF technique lacks sensitivity. This observation, which establishes for all photo-excited levels in <sup>28</sup>Si and the one photo-excited level in <sup>24</sup>Mg an isoscalar character, distinguishes these levels from the isovector GDR. An interesting observation is the isovector (dominated) nature of the 8904-keV level in <sup>26</sup>Mg. Apart from the unobserved 8904keV level, for  $^{28}$ Si the observed B(E1)-strength distributions resembles the excitation pattern obtained in  $(\alpha, \alpha')$ .

Considering the structure of the observed  $J^{\pi}=1^-$  levels, in the investigated mass region the absence of an intruder unique-parity subshell in the oscillator shell prevents valence-shell negative parity excitations built on n-particle n-hole ( $n \geq 2$ ) excitations. Hence, negative parity excitations involve solely cross oscillator shell 1-particle 1-hole excitations. In  $^{28}$ Si these are particle excitations from the  $1p_{1/2}$ - and  $1p_{3/2}$ - subshells to the unoccupied  $2s_{1/2}$ + and  $1d_{3/2}$ + orbitals in the sd shell or excitations of the valence particles in the fully occupied  $2d_{5/2}$ + orbitals to the fp shell, especially the spin-orbit lowered  $1f_{7/2}$ - subshell. Evaluating the shell



Eur. Phys. J. A (2025) 61:186 Page 11 of 15 186

**Table 5** Comparison of the level half-lives determined in this work,  $T_{1/2}$ , and found in the NNDC database [4],  $T_{1/2,lit}$ . If only a lower-limit is given, the level was recognised to be fed from higher-lying levels

$E_l$ [keV]	$J_i^\pi$	T <sub>1/2</sub> [fs]	$T_{1/2,lit}$ [fs]
1779.2(1)	2+	> 66	475(17)
7380.5(4)	2+	> 1.7	5(2)
7417.4(6)	2+	> 4.6	29(3)
7933.5(6)	2+	> 6.8	11(2)
8259.6(11)	2+	> 2.6	10(2)
8328.4(9)	1+	> 1.7	347(166)
9381.3(9)	2+	> 0.34	1.1(3)
$9479.1(11)^a$	2+	7.1(12)	6(2)
9495.9(6)	1+	> 1.3	5(2)
9795.3(12)	$(2^{+})$	> 5	
9929.5(4)	1-	$0.63(9)^a$	
10514.4(13)	$(2^{+})$	1.7(2)	
10595.3(5)	1+	0.34(4)	0.388(83)
10725.1(8)	1+	0.64(5)	0.624(110)
10900.1(5)	1+	0.10(1)	0.083(7)
10993.8(13)	1-	1.0(2)	
11295.4(15)	1-	1.8(6)	
11432.6(10)	$(2^{+})$	0.29(3)	< 21
11445.7(7)	1+	0.022(2)	0.0176(8)
12330.2	1(+)	0.12(3)	

<sup>&</sup>lt;sup>a</sup>Assuming there is no feeding

structure using the data from particle-transfer experiments to the odd-mass neighbors, e.g. see Refs. [59–61], reveals for both protons and neutrons an approximate 1 to 2 MeV wide gap between the  $1d_{5/2}$  and  $2s_{1/2}$  subshells and a gap of approximately 3 MeV between the  $1d_{5/2}$  and  $1d_{3/2}$  spin-orbit partner orbitals. The energy difference between the  $1d_{5/2}$ subshell at the Fermi level and the  $1p_{1/2}$  and  $1p_{3/2}$  subshells of the lower-lying oscillator shell amounts to  $\approx 4$  MeV and  $\approx 5.5 - 6$  MeV, respectively. For protons the  $f_{7/2}$  subshell is found at  $\approx 5.5$  MeV in <sup>29</sup>P, while in <sup>27</sup>Al the energy difference is  $\approx 7.9$  MeV. Adding the pairing energy, the negative-parity excitation can be expected to be found above 8 MeV. Indeed the data contained in the NNDC database [4], extracted from particle-transfer data, e. g. Refs. [62,63], locates for <sup>28</sup>Si the first negative parity  $J^{\pi} = 3^{-}$  level at 6879 keV, followed by two levels at 8413 keV with  $J^{\pi} = 4^{-}$ and 8905 keV with  $J^{\pi} = 1^{-}$ . The latter was not observed in this work. This is due to the low E1 strength and the fact that both known γ-ray decays at 7123-keV and 8902keV are in the proximity of intense transitions at 7115 keV (<sup>16</sup>O) and 8916-keV (<sup>11</sup>B), respectively, which might obscure these low-intensity transitions. The  $J^{\pi} = 1^{-}$  9929 keV level, which is the first 1<sup>-</sup> level observed in this work, is

surrounded by a group of levels at 9702 keV with  $J^{\pi} = (5^{-})$ , at 9764.5 keV with  $J^{\pi} = (3^{-})$ , and at 10182 keV with  $J^{\pi} = (3^{-})$ . With the exception of the 9702-keV level, the  $^{27}$ Al( $^{3}$ He, d) reaction [62] ascribes to all these levels a mixed l transfer of 1 + 3. The 9702 keV  $J^{\pi} = 5^{-}$  state has a sole l=3 transfer and can be identified as resulting from a proton  $[(1d_{5/2^+})^{-1}, 1f_{7/2^-}]$  configuration. Interestingly, in the particle-hole channel this configuration is expected to result in the odd-spin members of the multiplet to be settled near the energy of the particle-hole excitation, while the evenspin members are shifted to higher energies [64,65]. However, apart from the (relatively) pure  $J^{\pi} = 5^{-}$  member, the comparatively low spectroscopic factors of the other levels indicate that this two-particle excitation is fragmented due to mixing with other levels of the same spin and parity but different microscopic origin. For the 9929-keV 1<sup>-</sup> level, the low spectroscopic factors for l = 1 and l = 3 transfer in the  $^{27}$ Al( $^{3}$ He, d) reaction contradicts an assignment as member of the  $[(d_{5/2}+)^{-1}, f_{7/2}]$  multiplet. There is a variety of possibilities that can explain these low spectroscopic factors such as the level is based on a proton particle-hole excitation, it is a pure neutron excitation, or has a collective nature. Since there is no particle transfer data starting from <sup>27</sup>Si and <sup>29</sup>P, the first two possibibilities cannot be ruled out.

Usually the lowest lying 1<sup>-</sup> level in a nucleus results from quadrupole-octupole coupling and the deformation of the ground state can be assessed by the ordering of the first excited 3<sub>1</sub> and 1<sub>1</sub> levels. For a deformed nucleus, the interplay of the octupole phonon and the quadrupole deformation is sufficient to generate quadrupole-octupole coupled 1 levels. These are the bandheads and the K=0 and K=1octupole bands and found below the 3<sup>-</sup> band members. In <sup>28</sup>Si the first excited negative parity state is a 3<sup>-</sup> level and lies well below the first 1<sup>-</sup> state at 8905-keV, which was not observed in this work. This observation suggests a spherical nature for <sup>28</sup>Si. In contrast, <sup>24</sup>Mg ( $E_{3_1^-}$ : 7616 keV,  $E_{1_1^-}$ : 7555 keV) [66] and  $^{26}$ Mg ( $E_{3_1}$ : 6876 keV,  $E_{1_1}$ : 7062 keV) [67] have almost degenerate energies for the first excited  $3_1^-$  and  $1_1^-$  levels, which indicates considerable quadrupole correlations in the ground state of these nuclei. In a nearspherical nucleus the coupling of the octupole phonon with the quadrupole phonon results in a quintuplet of negative parity states with  $J^{\pi} = 1^{-}$  to  $5^{-}$  [12,68] at the sum energy of the two coupling phonons. For <sup>28</sup>Si the sum energy is 8656 keV, which is close to the unobserved 8904-keV level. An experimental energy of the quadrupole-octupole coupled 1<sup>-</sup> state higher than the sum energy is usually only observed near doubly-magic nuclei [68], where the low collectivity results in an enhanced blocking of configurations participating in the collective wavefunction of the other phonon. Indeed, the shell structure of <sup>28</sup>Si can be seen as resembling a doubly-magic nucleus, especially since the next subshell to both Fermi level



186 Page 12 of 15 Eur. Phys. J. A (2025) 61:186

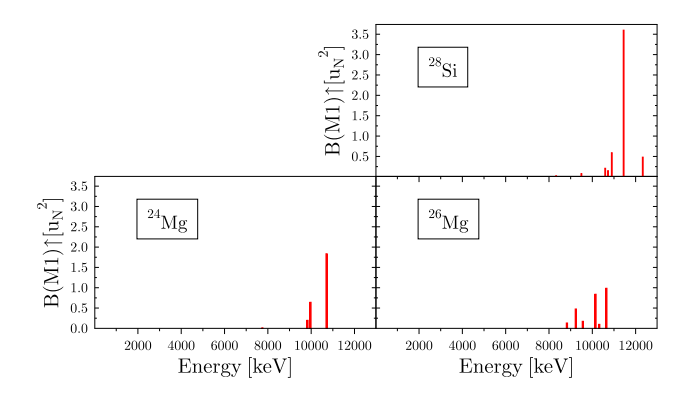
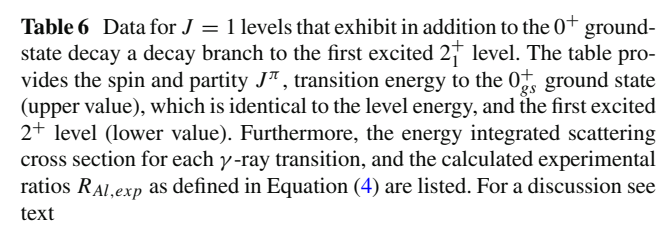


**Fig. 6** Systematics of the  $B(M1, 0_{gs}^+ \to 1^+)$  excitation strength for the nuclei <sup>24</sup>Mg [6], <sup>26</sup>Mg [8], and <sup>28</sup>Si. The plot is arranged according to the relative position of the nuclei in the Segre chart. The observed patterns resemble the results presented in Ref. [34]

containing, fully-occupied  $d_{5/2}$  subshells is  $s_{1/2}+$ . However, the absence of the other  $J^{\pi}=2^-$  and  $4^-$  members of the quadrupole-octupole coupled two-phonon multiplet renders such an interpretation for the 8904-keV state and the higherlying 9929-keV levels unlikely. Consequently, a one-particle one-hole nature of these states is more likely, but awaits confirmation from transfer experiments.

For a rigid rotor, the decay behaviour of excited J=1 states can be used to assign K quantum numbers by using the branching ratio as defined in Eq. 4. The calculated values are provided in Table 6. No tendency to agree with the theoretical values for  $R_{Al}=2$  for K=0 or  $R_{Al}=0.5$  for K=1 [39] is recognisable. This failure of the Alaga-rules indicates that its condition of a well-deformed rotor is not fulfilled and, consequently,  $^{28}$ Si cannot be treated as such.

Compared with the  $B(M1, 0^+ \rightarrow 1^-)$  values previously obtained in the  $(\gamma, \gamma')$  reaction by Berg et al. [34], the values extracted in this work are in general about 10 % lower; however, that is well within the uncertainties of both measurements. Figure 6 shows the resulting M1 strength distribution together with those for <sup>24</sup>Mg [6] and <sup>26</sup>Mg [8] measured at  $\gamma$ ELBE under similar conditions. The pattern of the first noticably excited  $1^+$  states of the two N = Znuclei <sup>24</sup>Mg and <sup>28</sup>Si are quite similar. The two major differences are a  $\approx 700$  keV higher excitation energy in <sup>28</sup>Si and that the strongest excited level 1<sup>+</sup> level in <sup>28</sup>Si  $[B(M1, 0^+ \rightarrow 1^+) = 3.6(4)\mu_N^2]$  is twice as strongly excited when compared to the corresponding level in <sup>24</sup>Mg  $[B(M1, 0^+ \to 1^+) = 1.8(5)\mu_N^2]$ . Furthermore, the comparison to a recent (p, p') experiment [17,18] reveals that the isoscalar 1+ levels are only extremely weakly populated in photon scattering. Interestingly, in <sup>28</sup>Si the strongest excited 1<sup>+</sup> state decays, apart from a newly observed weak branch to the first excited 2<sup>+</sup> level, exclusively to the ground state. This observation is in contrast to <sup>24</sup>Mg, for which the strongest excited 1<sup>+</sup> state at 10712 keV exhibits four decays to lower-



$J_l^\pi$	$E_{\gamma}$ [keV]	$I_{S,f}$ [eV·b]	$R_{Al,exp}$
1+	8328.8(10)	4.1(9)	2.6(16)
	6547.8(21)	5.1(22)	
1-	9929.7(7)	36(4)	0.20(7)
	8149.7(12)	4(1)	
1+	10596.7(12)	78(7)	0.13(6)
	8813.7(13)	6(2)	
1+	10900.4(11)	182(12)	0.84(11)
	9121.2(12)	90(6)	
1-	10993.6(15)	36(5)	0.15(8)
	9215.2(25)	3.2(13)	
1-	11296.4(13)	11(3)	0.76(51)
	9516.4(14)	5(2)	
1+	11446.2(8)	1820(90)	0.011(3)
	9665.5(12)	12(3)	
1(+)	12330.2(8)	250(20)	0.10(3)
	10550.4(12)	15(4)	

lying excited states, including one to the first excited  $0_2^+$  state. Instead in  $^{28}$ Si the two lower-lying, weaker excited levels at 10595 keV and 10900 keV exhibit decays to the first excited  $0_2^+$  level, while for the corresponding levels in  $^{24}$ Mg at 9829 keV and 9968 keV exclusively decays to the ground state and first excited  $2_1^+$  level were observed. Consequently, the addition of two protons and two neutrons to fill the respective  $d_{5/2^+}$  subshells preserves the pattern of the M1 excitation strength but inverts the decay behaviour with respect to the first excited  $0^+$  state.

In Ref. [43] it is stated, that Ref. [69] assigned an oblate character to the  $0^+_{gs}$  ground state and Ref. [70] a prolate character for the band built upon the first excited  $0^+_2$  state. The considerable  $10^3 \times \rho^2(E0) = 262(31)$  value [41] for the  $0^+_2 \to 0+_{gs}$  transition indicates a considerable difference of the  $\beta$  deformation parameters as well as significant mixing between the two  $0^+$  states. In Ref. [6] the branching ratio of the strongest excited  $1^+$  state to the  $0^+_{gs}$  ground state and the first excited  $0^+_2$  state was used to extract mixing parameters and, subsquently, when using the  $\rho^2(E0)$  value the difference in quadrupole deformation. However, as outlined in Ref. [44] this method relies on the assumption that the photo-excited level is a pure particle-hole excitation. Using the two-state mixing formalism [43], the wave functions of the observed



Eur. Phys. J. A (2025) 61:186 Page 13 of 15 186

**Table 7** Data for  $1^+$  levels that decay to the  $0_{gs}^+$  ground state and the first excited  $0_2^+$  state. Given are the  $\gamma$ -ray energies,  $E_{\gamma}$ , from which the highest corresponds to the level energy, the integrated scattering cross section,  $I_{S,f}$ , the branching ratio,  $R_0$ , as defined in Eq. 7, the mixing amplitudes  $\cos \alpha$  and  $\sin \alpha$ , and the resulting difference in deformation according to Eq. 6. For a discussion see text

$E_{\gamma}$ [keV]	$I_{S,f}$ [eV·b]	$R_0$	$\cos \alpha$	$\Delta(\beta_2)^2$
10596.7(12) 5615.6(6)	78(7) 15(2)	1.29(29)	0.44(6)	0.15(6)
10900.1(5) 5919.8(7)	184(12) 8(2)	0.27(9)	0.79(6)	0.19(9)

states are given as linear combinations of the pure oblate  $0^+_{obl}$  and prolate  $0^+_{prol}$  state

$$|0_{gs}^{+}\rangle = \cos \alpha |0_{obl}^{+}\rangle + \sin \alpha |0_{prol}^{+}\rangle$$

$$|0_2^+\rangle = -\sin\alpha |0_{obl}^+\rangle + \cos\alpha |0_{prol}^+\rangle.$$

As outlined in Ref. [44], if a 1<sup>+</sup> level corresponds to a one-particle one-hole excitation built upon the structure of the ground state, the observed decay to the  $0_2^+$  level corresponds to the decay to the oblate  $|0_{obl}^+\rangle$  component mixed into this level. Hence, the ratio of the mixing amplitudes  $\sin\alpha$  and  $\cos\alpha$  can be extracted from the experimental ratio  $R_0$  of the  $B(\Pi 1)$  reduced transition strengths

$$R_0 = \frac{B(M1, 1_i^+ \to 0_2^+)}{B(M1, 1_i^+ \to 0_{gs}^+)} = \frac{I_{S, 0_2^+}}{I_{S, 0_{gs}^+}} \cdot \frac{E_{\gamma, 0_{gs}^+}^3}{E_{\gamma, 0_2^+}^3} = \left[\frac{\sin \alpha}{\cos \alpha}\right]^2.$$

Here, in the determination of the  $B(\Pi 1)$  strength, the branching ratio of ground-state decay width  $\Gamma_0$  to total decay width,  $\Gamma$ , enters the calculation of both decay strengths and, therefore, the uncertainties of both associated with the other  $\gamma$  rays depopulating the level of interest enter. To prevent these additional uncertainties entering the final value, the ratio  $R_0$  can be transformed in such a way that the integrated scattering cross sections  $I_{S,f}$  with smaller relative uncertainties enter together with the  $\gamma$ -ray energies  $E_{\gamma,f}$ . For  $^{28}$ Si, the  $1^+$  levels at 10595.3(5) keV and 10900.1(5) keV as well as the  $1^-$  level at 9929.5(4) keV exhibit decays to the  $0_{gs}^+$  ground state and the  $0_2^+$  level.

This approach results in mixing amplitudes of  $\cos \alpha$  and  $\sin \alpha$  shown in Table 7, which, when neglecting any form of triaxiality, enter the equation (taken from Ref. [43])

$$\rho^2(E0) = \left(\frac{3Z}{4\pi}\right)^2 \cos^2 \alpha \cdot \sin^2 \alpha \left(\beta_{2,obl}^2 - \beta_{2,prol}^2\right)^2.$$

Here, Z is the proton number and  $\beta_{2,obl}$  and  $\beta_{2,prol}$  are the quadrupole deformation parameters of the oblate deformed ground state  $0_{obl}^+$  and the prolate deformed  $0_{prol}^+$  state, respectively. Using the experimental value  $1000 \times \rho^2(E0) =$ 262(31) [41] and the amplitudes extracted from this work, the difference  $\Delta \beta_{2,i}^2$  in  $\beta_{2,i}^2$  is calculated as indicated in Table 7. The two 1<sup>+</sup> levels that exhibit a decay branch to the 0<sup>+</sup> state deliver a set of inconsistent values. This raises the question about the validity of the assumption of the states being pure particle-hole excitations built upon the ground state. Since the set of available particle-transfer experiments [4] allows only to extract information about proton-particle states  $[^{27}Al(^{3}He,d)]$  of neutron-hole states  $[^{29}Si(p,d)]$ , but not for proton-hole or neutron-particle states, it is not possible to judge which of the two levels fulfills the criteria. It appears, that both 1<sup>+</sup> levels at 10595 keV and 10900 keV do have admixtures of the by far strongest excited 1<sup>+</sup> level at 11446 keV in their wave functions, which enhances the ground-state decay branch and obscures the crucial branching ratio. Indeed the 10900-keV level, which is closer to the 11446-keV level, has a larger ground-state branching ratio. However, at the present level of information it is not possible to judge whether one of these two levels fulfills the criteria of a pure particle-hole excitation. Furthermore, for both states the low intensity of the branching transition results in a comparably high relative uncertainty, which exceeds the sensitivity of the method.

## 5 Summary

The present  $^{28}\mathrm{Si}(\gamma,\gamma')$  experiment revealed several previously unknown lifetimes for J=1 states that are relevant for nucleosynthesis processes. A negligible amount of E1 strength was observed that exhausts only 0.026(2)% of the energy-weighted sum rule. A comparison to inelastic  $\alpha$ -particle scattering attributes an isoscalar character to all observed  $1^-$  levels. This result afirms the connection of sizable low-lying isoscalar E1 strength and an excess of one species of nucleons. In comparison to a previous  $(\gamma, \gamma')$  experiment, this work provides a  $\approx 10\%$  reduced M1 strength; however, this in well within the experimental uncertainty. Furthermore, a branching ratio based method raises doubts that  $^{28}\mathrm{Si}$  has any noticable deformation in its ground state.

Acknowledgements The collaboration is indebted to the ELBE accelerator crew for the excellent electron beams. The members of the UWS Nuclear Physics Research Group acknowledge financial support from the UK Science and Technology Facilities Council (STFC, Grant No. ST/P005101/1). D. K., K. G., and G. R. acknowledge support by the European Union – Next Generation EU, through the National Recovery and Resilience Plan of the Republic of Bulgaria, project No. BG-RRP-2.004-0008-C01, and by the Bulgarian Ministry of Education and Sci-



186 Page 14 of 15 Eur. Phys. J. A (2025) 61:186

ence, within the National Roadmap for Research Infrastructures (object CERN).

**Data availability statement** Data will be made available on reasonable request. [Author's comment: The datasets generated during and/or analysed during the current study are available from the corresponding author on reasonable request.].

Code availibility statement This manuscript has no associated code/ software. [Author's comment: Code/Software sharing not applicable to this article as no code/software was generated or analysed during the current study.].

**Open Access** This article is licensed under a Creative Commons Attribution 4.0 International License, which permits use, sharing, adaptation, distribution and reproduction in any medium or format, as long as you give appropriate credit to the original author(s) and the source, provide a link to the Creative Commons licence, and indicate if changes were made. The images or other third party material in this article are included in the article's Creative Commons licence, unless indicated otherwise in a credit line to the material. If material is not included in the article's Creative Commons licence and your intended use is not permitted by statutory regulation or exceeds the permitted use, you will need to obtain permission directly from the copyright holder. To view a copy of this licence, visit http://creativecommons.org/licenses/by/4.0/.

# References

- I.J. Thompson, F.M. Nunes, Nuclear Reactions for Astrophysics (Cambridge University Press, Cambridge, 2009)
- S.G. Ryan, A.J. Norton, Stellar Evolution and Nucleosynthesis (Cambridge University Press, Cambridge, 2010)
- 3. C. Bertulani, P. Danielewicz, *Introduction to Nuclear Reactions* (CRC Press, Boca Raton, 2021)
- 4. M. Shamsuzzoha Basunia, Nucl. Data Sheets 114, 1189 (2013)
- P. Adsley, A.M. Laird, Z. Meisel, Phys. Rev. C 102, 015801 (2020). https://doi.org/10.1103/PhysRevC.102.015801
- J. Deary, M. Scheck, R. Schwengner, D. O'Donnell, D. Bemmerer, R. Beyer, Th. Hensel, A.R. Junghans, T. Kögler, S.E. Müller, K. Römer, K. Schmidt, S. Turkat, S. Urla"s, A. Wagner, M. Bowry, P. Adsley, O. Agar, R. Chapman, F.C.L. Crespi, D.T. Doherty, U. Friman Gayer, R.-D. Herzberg, J. Isaak, R.V.F. Janssens, T. Kröll, B. Löher, B.S. Nara Singh, P. von Neumann-Cosel, L. Pellegri, E.E. Peters, G. Rainovski, D. Savran, J.F. Smith, M. Spieker, P.G. Thirolf, S. Triambak, W. Tornow, M. Venhart, M. Wiedeking, O. Wieland, S.W. Yates, A. Zilges, Eur. Phys. Jour. A 59, 198 (2023). https://doi.org/10.1140/epja/s10050-023-01111-7
- J. Sinclair, M. Scheck, S.W. Finch, Krishichayan, U. Friman-Gayer, W. Tornow, G. Battaglia, T. Beck, R. Chapman, M.M.R. Chishti, Ch. Fransen, R. Gonzales, E. Hoemann, J. Isaak, R.V.F. Janssens, D.A. Jaroszynski, S. Johnson, M.D. Jones, J.M. Keatings, N. Kelly, J. Kleemann, D. Little, B. Löher, K.R. Mashtakov, M. Müscher, D. O'Donnell, O. Papst, E.E. Peters, D. Savran, M. Schilling, R. Schwengner, P. Spagnoletti, M. Spieker, V. Werner, J. Wilhelmy, O. Wieland, S.W. Yates, A. Zilges, Eur. Phys. Jour. A 56, 105 (2020). https://doi.org/10.1140/epja/s10050-020-00118-8
- R. Schwengner, A. Wagner, Y. Fujita, G. Rusev, M. Erhard, D. De Frenne, E. Grosse, A.R. Junghans, K. Kosev, K.D. Schilling, Phys. Rev. C 79, 037303 (2009). https://doi.org/10.1103/PhysRevC.79. 037303
- R.J. deBoer, M. Wiescher, J. Görres, R. Longland, C. Iliadis, G. Rusev, A.P. Tonchev, Phys. Rev. C 82, 025802 (2010). https://doi.org/10.1103/PhysRevC.82.025802

- U. Kneissl, H.H. Pitz, A. Zilges, Prog. Part. Nucl. Phys. 37, 349 (1996). https://doi.org/10.1016/0146-6410(96)00055-5
- A. Zilges, D.L. Balabanski, J. Isaak, N. Pietralla, Prog. Part. Nucl. Phys. 122, 103903 (2022). https://doi.org/10.1016/j.ppnp.2021. 103903
- U. Kneissl, N. Pietralla, A. Zilges, J. Phys. G 32, R217 (2006). https://doi.org/10.1016/j.ppnp.2021.103903
- K. Heyde, P. von Neumann-Cosel, A. Richter, Rev. Mod. Phys. 82, 2365 (2010). https://doi.org/10.1103/RevModPhys.82.2365
- P.F. Bortignon, A. Bracco, R.A. Broglia, Giant Resonances (Harwood Academic Publishers, New York, 1998)
- M. Harakeh, A. van der Woude, Giant Resonances (Oxford University Press, Oxford, 2001)
- K. Langanke, G. Martinez-Pinedo, P. von Neumann-Cosel, A. Richter, Phys. Rev. Lett. 93, 202501 (2004). https://doi.org/10. 1103/PhysRevLett.93.202501
- H. Matsubara, A. Tamii, H. Nakada, T. Adachi, J. Carter, M. Dozono, H. Fujita, K. Fujita, Y. Fujita, K. Hatanaka, W. Horiuchi, M. Itoh, T. Kawabata, S. Kuroita, Y. Maeda, P. Navratil, P. von Neumann-Cosel, R. Neveling, H. Okamura, L. Popescu, I. Poltoratska, A. Richter, B. Rubio, H. Sakaguchi, S. Sakaguchi, Y. Sakemi, Y. Sasamoto, Y. Shimbara, Y. Shimizu, F.D. Smit, K. Suda, Y. Tameshige, H. Tokieda, Y. Yamada, M. Yosoi, J. Zenihiro, Phys. Rev. Lett. 115, 102501 (2015). https://doi.org/10.1103/PhysRevLett.115.102501
- H. Matsubara, A. Tamii, Front. Astron. Space Sci. 8, 667058 (2021). https://doi.org/10.3389/fspas.2021.667058
- J. Ahrens, H. Borchert, K.H. Czock, H.B. Eppler, H. Gimm, H. Gundrum, M. Kröning, P. Riehn, G. Sita Ram, A. Zieger, B. Ziegler, Nucl. Phys. A 251, 479 (1975). https://doi.org/10.1016/0375-9474(75)90543-6
- H. Harada, K. Furutaka, H. Ohgaki, H. Toyokawa, J. Nucl. Sci. Tech. 38, 465 (2001). https://doi.org/10.1080/18811248.2001. 9715055
- D. Savran, T. Aumann, A. Zilges, Prog. Part. Nucl. Phys. 70, 210 (2013). https://doi.org/10.1016/j.ppnp.2013.02.003
- A. Bracco, E.G. Lanza, A. Tamii, Prog. Part. Nucl. Phys. 106, 360 (2019). https://doi.org/10.1016/j.ppnp.2019.02.001
- E.G. Lanza, L. Pellegri, A. Vitturi, M.V. Andres, Prog. Part. Nucl. Phys. 129, 104006 (2023). https://doi.org/10.1016/j.ppnp.2022. 104006
- V.O. Nesterenko, A. Repko, J. Kvasil, P.-G. Reinhard, Phys. Rev. Lett. 120, 182501 (2018). https://doi.org/10.1103/PhysRevLett. 120.182501
- V.O. Nesterenko, A. Repko, J. Kvasil, P.-G. Reinhard, Phys. Rev. C 100, 064302 (2019). https://doi.org/10.1103/PhysRevC. 100.064302
- P. von Neumann-Cosel, V.O. Nesterenko, I. Brandherm, P.I. Vishnevskiy, P.-G. Reinhard, J. Kvasil, H. Matsubara, A. Repko, A. Richter, M. Scheck, A. Tamii, Phys. Rev. Lett. 133, 232502 (2025). https://doi.org/10.1103/PhysRevLett.133.232502
- T. Hartmann, J. Enders, P. Mohr, K. Vogt, S. Volz, A. Zilges, Phys. Rev. C 65, 034301 (2002). https://doi.org/10.1103/PhysRevC.65. 034301
- M. Spieker, A. Heusler, B.A. Brown, T. Faestermann, R. Hertenberger, G. Potel, M. Scheck, N. Tsoneva, M. Weinert, H.-F. Wirth, A. Zilges, Phys. Rev. Lett. 125, 102503 (2020). https://doi.org/10.1103/PhysRevLett.125.102503
- L.I. Schiff, Phys. Rev. 83, 252 (1951). https://doi.org/10.1103/ PhysRev.83.252
- R. Moreh, W.C. Sellyey, R. Vodhanel, Phys. Rev. C 22, 1820 (1980). https://doi.org/10.1103/PhysRevC.22.1820
- G. Rusev, A.P. Tonchev, R. Schwengner, C. Sun, W. Tornow, Y.K.
   Wu, Phys. Rev. C 79, 047601 (2009). https://doi.org/10.1103/ PhysRevC.79.047601



Eur. Phys. J. A (2025) 61:186 Page 15 of 15 186

 J.H. Kelley, C.G. Sheu, Nucl. Phys. A 880, 88 (2012). https://doi. org/10.1016/j.nuclphysa.2012.01.010

- D. Gribble, C. Iliadis, R.V.F. Janssens, U. Friman-Gayer, Krishichayan, S. Finch, Phys. Rev. C 106, 014308 (2022). https://doi.org/10.1103/PhysRevC.106.014308
- U.E.P. Berg, K. Ackermann, K. Bangert, C. Bläsing, W. Naatz,
   R. Stock, K. Wienhard, M.K. Brussel, T.E. Chapuran, B.H.
   Wildenthal, Phys. Lett. B 140, 191 (1984). https://doi.org/10.1016/ 0370-2693(84)90918-3
- P. Adsley, V.O. Nesterenko, M. Kimura, L.M. Donaldson, R. Neveling, J.W. Brümmer, D.G. Jenkins, N.Y. Kheswa, J. Kvasil, K.C.W. Li, D.J. Marin-Lambarri, Z. Mabika, P. Papka, L. Pellegri, V. Pesudo, B. Rebeiro, P.G. Reinhard, F.D. Smit, W. Yahia-Cherif, Phys. Rev. C 103, 044315 (2021). https://doi.org/10.1103/PhysRevC.103.044315
- D.G. Jenkins, C.J. Lister, M.P. Carpenter, P. Chowdury, N.J. Hammond, R.V.F. Janssens, T.L. Khoo, T. Lauritsen, D. Seweryniak, T. Davinson, P.J. Woods, A. Jokinen, H. Penttila, F. Haas, S. Courtin, Phys. Rev. C 86, 064308 (2012). https://doi.org/10.1103/PhysRevC.86.064308
- P. Adsley, D.G. Jenkins, J. Cseh, S.S. Dimitrova, J.W. Brümmer, K.C.W. Li, D.J. Marin-Lambarri, K. Lukyanov, N.Y. Kheswa, R. Neveling, P. Papka, L. Pellegri, V. Pesudo, L.C. Pool, G. Riczu, F.D. Smit, J.J. van Zyl, E. Zemlyanaya, Phys. Rev. C 95, 024319 (2017). https://doi.org/10.1103/PhysRevC.95.024319
- G. Alaga, K. Alder, A. Bohr, B.R. Mottelson, K. Dan, Vidensk. Selesk. Mat. Fys. Medd. 29, 1 (1955)
- D. Savran, S. Müller, A. Zilges, M. Babilon, M.W. Ahmed, J.H. Kelley, A. Tonchev, W. Tornow, H.R. Weller, N. Pietralla, J. Li, I.V. Pinayev, Y.K. Wu, Phys. Rev. C 71, 034304 (2005). https://doi.org/10.1103/PhysRevC.71.034304
- A. Nakada, Y. Torizuka, J. Phys. Soc. Jpn. 32, 1 (1972). https://doi. org/10.1143/JPSJ.32.1
- T. Kibedi, R.H. Spear, At. Data Nucl. Data Tables 89, 77 (2005). https://doi.org/10.1016/j.adt.2004.11.002
- K. Heyde, J.L. Wood, Rev. Mod. Phys. 83, 1467 (2011). https://doi.org/10.1103/RevModPhys.83.1467
- P.E. Garrett, M. Zielinska, E. Clement, Prog. Part. Nucl. Phys. 124, 103931 (2022). https://doi.org/10.1016/j.ppnp.2021.103931
- 44. G. Rusev, R. Schwengner, F. Dönau, S. Frauendorf, L. Käubler, L.K. Kostov, S. Mallion, K.D. Schilling, A. Wagner, E. Grosse, H. von Garrel, U. Kneissl, C. Kohstall, M. Kreutz, H.H. Pitz, M. Scheck, F. Stedile, P. von Brentano, J. Jolie, A. Linnemann, N. Pietralla, V. Werner, Phys. Rev. Lett. 95, 062501 (2005). https:// doi.org/10.1103/PhysRevLett.95.062501
- B. Löher, V. Derya, T. Aumann, J. Beller, N. Cooper, M. Duchene, J. Endres, E. Fiori, J. Isaak, J. Kelley, M. Knörzer, N. Pietralla, Ch. Romig, D. Savran, M. Scheck, H. Scheit, J. Silva, A. Tonchev, W. Tornow, H. Weller, V. Werner, A. Zilges, Nucl. Inst. Meth. A 723, 136 (2013). https://doi.org/10.1016/j.nima.2013.04.087
- R. Schwengner, R. Beyer, F. Dönau, E. Grosse, A. Hartmann, A.R. Junghans, S. Mallion, G. Rusev, K.D. Schilling, W. Schulze, A. Wagner, Nucl. Instrum. Methods A 555, 211 (2005). https://doi.org/10.1016/j.nima.2005.09.024
- GEANT4 collaboration, Nucl. Instrum. Meth. A 506, 250 (2003). https://doi.org/10.1016/S0168-9002(03)01368-8
- R. Schwengner, R. Massarczyk, R. Beyer, N. Benouaret, A. Ferrari, A. Hartmann, T. Hensel, E. Masha, S.E. Müller, K. Römer, M. Scheck, K. Schmidt, S. Turkat, S. Urla"s, A. Wagner, A. Yadav, Phys. Rev. C 111, 014312 (2025). https://doi.org/10.1103/PhysRevC.111.014312

- D.R. Tilley, H.R. Weller, C.M. Cheves, Nucl. Phys. A 564, 1 (1993). https://doi.org/10.1016/0375-9474(93)90073-7
- C.E. Moss, J.D. Sherman, Nucl. Phys. A 259, 413 (1976). https://doi.org/10.1016/0375-9474(76)90076-2
- J.W. Maas, E. Somorjai, H.D. Graber, C.A. Van Den Wijngaart, C. Van Der Leun, P.M. Endt, Nucl. Phys. A 301, 213 (1978). https://doi.org/10.1016/0375-9474(78)90263-4
- P.M. Endt, Nucl. Phys. A 521, 1 (1990). https://doi.org/10.1016/ 0375-9474(90)90598-G
- P.M. Endt, Nucl. Phys. A 633, 1 (1998). https://doi.org/10.1016/ S0375-9474(97)00613-1
- E. Strandberg, R. Azuma, M. Beard, L. Buchmann, H. Costantini, M. Couder, A. Couture, S. Falahat, J. Görres, P.J. LeBlanc, H.Y. Lee, S. O'Brien, A. Palumbo, M. Pignatari, K. Scheller, E. Stech, W.P. Tan, C. Ugalde, M. Wiescher, Phys. Rev. C 77, 055801 (2008). https://doi.org/10.1103/PhysRevC.77.055801
- A. Bohr, B.R. Mottelson, *Nuclear Structure*, vol. II (Benjamin, Reading, 1975)
- D. Savran, M. Babilon, A.M. van den Berg, M.N. Harakeh, J. Hasper, A. Matic, H.J. Wörtche, A. Zilges, Phys. Rev. Lett. 97, 172502 (2006). https://doi.org/10.1103/PhysRevLett.97.172502
- E.G. Lanza, A. Vitturi, E. Litvinova, D. Savran, Phys. Rev. C 89, 041601 (2014). https://doi.org/10.1103/PhysRevC.89.041601
- D. Savran, V. Derya, S. Bagchi, J. Endres, M.N. Harakeh, J. Isaak, N. Kalantar-Nayestanaki, E.G. Lanza, B. Löher, A. Najafi, S. Pascu, S.G. Pickstone, N. Pietralla, V.Y. Ponomarev, C. Rigollet, C. Romig, M. Spieker, A. Vitturi, A. Zilges, Phys. Lett. B 786, 16 (2018). https://doi.org/10.1016/j.physletb.2018.09.025
- R.L. Kozub, Phys. Rev. 172, 1078 (1968). https://doi.org/10.1103/ PhysRev.172.1078
- S. Piskor, W. Schäferlingova, Nucl. Phys. A 510, 301 (1990). https://doi.org/10.1016/0375-9474(90)90241-D
- W.W. Dykoski, D. Dehnhard, Phys. Rev. C 13, 80 (1976). https://doi.org/10.1103/PhysRevC.13.80
- H. Nann, Nucl. Phys. A 376, 61 (1982). https://doi.org/10.1016/ 0375-9474(82)90533-4
- G.J. Wagner, Nucl. Phys. A 176, 47 (1971). https://doi.org/10. 1016/0375-9474(71)90730-5
- A. deShalit, I. Talmi, Nuclear Shell Theory (Academic Press, New York, 1963)
- K.L.G. Heyde, The Nuclear Shell Model (Springer, Heidelberg, 1993)
- M. Shamsuzzoha Basunia, A. Chakraborty, Nucl. Data Sheets 186, 2 (2022). https://doi.org/10.1016/j.nds.2022.11.002
- M.S. Basunia, A.M. Hurst, Nucl. Data Sheets 134, 1 (2016). https://doi.org/10.1016/j.nds.2016.04.001
- W. Andrejtscheff, Ch. Kohstall, P. von Brentano, C. Fransen, U. Kneissl, N. Pietralla, H.H. Pitz, Phys. Lett. B 506, 239 (2001). https://doi.org/10.1016/S0370-2693(01)00340-9
- O. Häusser, T.K. Alexander, D. Pelte, B.W. Hooton, H.C. Evans, Phys. Rev. Lett. 23, 320 (1969). https://doi.org/10.1103/ PhysRevLett.23.320
- F. Glatz, P. Betz, J. Siefert, F. Heidinger, H. Röpke, Phys. Rev. Lett. 46, 1559 (1981). https://doi.org/10.1103/PhysRevLett.46.1559

